Bloch method for the analysis of modes in microstructured optical fibers

Boris T. Kuhlmey[1,2], **Ross C. McPhedran**[1] **and C. Martijn de Sterke**[1]

1: Centre for Ultrahigh-bandwidth Devices for Optical Systems (CUDOS) and School of Physics, University of Sydney 2006, Australia

2: Institut Fresnel UMR 6133 CNRS, Faculté des Sciences et Techniques de St. Jérôme, 131197 Marseille, France

borisk@physics.usyd.edu.au

Abstract: We discuss a transform technique for analyzing the wave vector content of microstructured optical fiber (MOF) modes, which is computationally efficient and gives good physical insight into the nature of the mode. In particular, if the mode undergoes a transition from a bound state to an extended state, this is evident in the spreading-out of its transform. The method has been implemented in the multipole formulation for finding MOF modes, but are capable of adaptation to other formulations.

OCIS codes: (060.2310) Fiber optics; (000.3860) Mathematical methods in physics

References and links

1. P. St J. Russell, "Photonic crystal fibers," Science **299**, 358-362 (2003).
2. C. M. Smith, N. Venkataraman, M. T. Gallagher, D. Muller, J. A. West, N. F. Borrelli, D. C. Allan, and K. W. Koch, "Low-loss hollow-core silica/air photonic bandgap fibre," Nature **424**, 657-659 (2003).
3. B. T. Kuhlmey, R. C. McPhedran, and C. M. de Sterke, "Modal cutoff in microstructured optical fibers," Opt. Lett., **27**, 1684-1686 (2002).
4. B. T. Kuhlmey, R. C. McPhedran, C. M. de Sterke, P. A. Robinson, G. Renversez, and D. Maystre, "Microstructured optical fibers: where's the edge?," Opt. Express,**10**, 1285-1290 (2002), http://www.opticsexpress.org/abstract.cfm?URI=OPEX-10-22-1285
5. N. A. Mortensen, "Effective area of photonic crystal fibers", Opt. Express **10**, 341-348 (2002), http://www.opticsexpress.org/abstract.cfm?URI=OPEX-10-7-341
6. T. P. White, B. T. Kuhlmey, R. C. McPhedran, D. Maystre, G. Renversez, C. M. de Sterke, and L. C. Botten, "Multipole method for microstructured optical fibers I: formulation," J. Opt. Soc. Am. B **19**, 2322-2330 (2002), and "Erratum," J. Opt. Soc. Am. B **20**, 1581 (2003).
7. B. T. Kuhlmey, T. P. White, G. Renversez, D. Maystre, L. C. Botten, C. M. de Sterke and R. C. McPhedran, " Multipole formulation for microstructured optical fibers II: implementation and results," J. Opt. Soc. Am. B **19**, 2331-2340 (2002).
8. http://www.physics.usyd.edu.au/cudos/mofsoftware/
9. T. A. Birks and J. C. Knight and St. J. Russel, "Endlessly single-mode photonic crystal fiber," Opt. Lett. **22** 961-963 (1997).
10. M. Reed and B. Simon, *Methods of Modern Mathematical Physics IV: Analysis of Operators* (Academic, New York, 1978).
11. G. Allaire, C. Conca and M. Vanninathan,"The Bloch Transform and applications," 29th Congress of Numerical Analysis, ESAIM: Proceedings **3**, 65-84 (1998), http://www.edpsciences.org/articlesproc/Vol.3/conca/conca.htm
12. P. R. McIsaac, "Symmetry-induced modal characteristics of uniform waveguides-I: Summary of results," IEEE Trans. Microwave Theory Tech. **MTT-23**, 421-429 (1975).

1. Introduction

There has been remarkable progress in recent years in the design and fabrication of microstructured optical fibers (MOFs) for a range of novel applications, such as dispersion compensation,

#3960 - $15.00 US Received 2 March 2004; revised 6 April 2004; accepted 8 April 2004

continuum generation and guiding of light in air [1, 2]. These advances have simultaneously profited from sophisticated numerical methods for the finding and analysis of the properties of modes in MOFs, and posed challenges to the developers of those methods. For example, the evaluation of mode number in MOFs is a more subtle question than in conventional fibers [3, 4, 5]. In investigations of transitions of modes which occur as the geometrical parameters of the MOF are changed at fixed wavelength, it may happen that the mode changes rapidly from being tightly bound to the central defect of the MOF, to being weakly bound by reflection off the edge of the microstructured region [4]. In such a case, it is important to be sure that the tightly and weakly bound modes are indeed related by a continuous, albeit rapid, transition process.

We discuss here a solution this challenge, which has proved effective within the context of studies using the multipole method [6, 7]. It is not only present in the multipole code, which is available for free download [8], but could also be easily implemented in other methods which can deliver accurate solutions for the electromagnetic fields of modes in MOFs.

2. Bloch transform of MOF modes

Among the variety of MOFs studied in the literature, those having a cladding consisting of inclusions situated on the nodes of a subset of a periodic lattice (*e.g.* photonic crystal cladding) have received most attention. Properties of such MOFs are closely linked to the band structure of their cladding, and popular models such as the effective index model for solid core MOFs are based on properties of the band structure [9]. Each point of a band diagram is associated with a Bloch wave in the periodic structure, and it would be most useful to be able to project MOF modes on the basis formed by these Bloch waves. We here use a discrete Fourier transform applied to the modal fields sampled over specific points along the structure – an optimized form of the transform we will refer to as the Bloch transform for simplicity – which is able to isolate Bloch components of a mode.

We consider a MOF with N_i inclusions centered around position vectors $\mathbf{c}_l$ ($l \in [1..N_\mathrm{i}]$). We assume that position vectors $\mathbf{c}_l$ describe a subset of an infinite periodic lattice $\mathscr{L}$. To form the Bloch transform of a given MOF mode, we choose a number of quantities $B_n(\mathbf{c}_l)$ characterizing the complex field amplitudes at each of the N_i inclusions. In the multipole formulation, it is natural to take these to be the amplitudes of the multipoles occurring in the expansions of E_z and H_z, but in other methods they could be simply the complex values of E_z and H_z at a small number of points in each inclusion. We then define the Bloch transform for quantity B_n by

$$\mathscr{B}_n(\mathbf{k}) = \sum_{l=1}^{N_\mathrm{i}} \exp(-i\mathbf{k}\cdot\mathbf{c}_l) B_n(\mathbf{c}_l) \; . \tag{1}$$

Note that the term "Bloch transform" is used otherwise in the context of the Floquet-Bloch theory by other authors, see *e.g.* Refs. [10, 11]. Although the Bloch transform we define here is not directly related to the one defined in Ref. [11], its properties – which come from the specific way of sampling the fields over the lattice of the structure – are similar in that they enable an analysis of fields in terms of Bloch components.

If a mode consists of a superposition of N_B Bloch waves with Bloch vectors $\mathbf{k}_\mathrm{B}^m$, so that its field distribution satisfies

$$V(\mathbf{r}) = \sum_{m=1}^{N_\mathrm{B}} \exp(i\mathbf{k}_\mathrm{B}^m\cdot\mathbf{r}) v_{\mathbf{k}_\mathrm{B}^m}(\mathbf{r}) \; , \tag{2}$$

where functions $v_{\mathbf{k}_\mathrm{B}^m}(\mathbf{r})$ have the periodicity of the lattice $\mathscr{L}$, quantities $B_n(\mathbf{c}_l)$ satisfy

$$B_n(\mathbf{c}_l) = \sum_{m=1}^{N_\mathrm{B}} \hat{B}_n^m \exp(i\mathbf{k}_\mathrm{B}^m\cdot\mathbf{c_l}) \; , \tag{3}$$

#3960 - $15.00 US Received 2 March 2004; revised 6 April 2004; accepted 8 April 2004

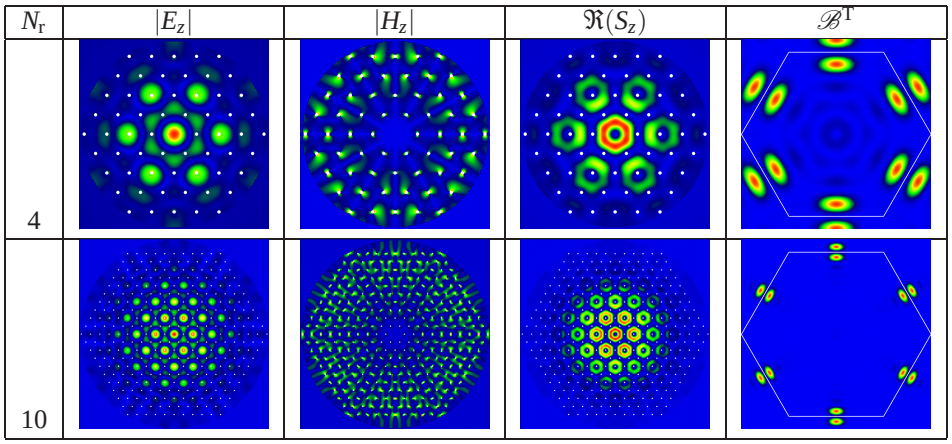

Fig. 1. Field maps and total Bloch transform of a mode consisting essentially of a superposition of 6 Bloch waves. Note that the fields are depicted in the direct space (**r**-space), whereas the Bloch transform is in the reciprocal space (**k**-space): the white hexagon on the Bloch transform map depicts the edges of the first Brillouin zone. Here $\Lambda = 2.3\ \mu$m, $\lambda = 1.55\ \mu$m, $d/\Lambda = 0.15$, and $n_{\text{silica}} = 1.44402036$.

where $\hat{B}_n^m$ is the complex amplitude of the Bloch wave associated with Bloch vector $\mathbf{k}_{\text{B}}^m$ in the decomposition of $B_n(\mathbf{c}_l)$. From Eqs. (1) and (3) it is then straightforward to see that $\mathscr{B}_n(\mathbf{k})$ peaks when $\mathbf{k} = \mathbf{k}_{\text{B}}^m$.

Further, Eq. (1) shows that the Bloch transform has the periodicity of the reciprocal lattice $\mathscr{L}^*$. Indeed the reciprocal lattice is defined by all vectors **G** such that

$$\forall \mathbf{c} \in \mathscr{L}, \mathbf{G} \cdot \mathbf{c} \in 2\pi\mathbb{Z}, \tag{4}$$

where $\mathbb{Z}$ is the set of all integers. Since the vectors $\mathbf{c}_l$ form a subset of $\mathscr{L}$, adding any vector **G** of $\mathscr{L}^*$ to **k** in Eq. (1) leaves the result unchanged. It is hence sufficient to compute the Bloch transform in the first Brillouin zone (FBZ) associated with $\mathscr{L}$.

For a given mode, the essential information in the Bloch transform may be captured by plotting a single $|\mathscr{B}_n(\mathbf{k})|$ as a function of **k**. If this is not the case, it may be convenient to form the *total Bloch transform*, by summing over the (appropriately normalized) transforms of all the representative quantities

$$\mathscr{B}^T(\mathbf{k}) = \sum_n \frac{1}{\sup_{\mathbf{k}' \in \mathbb{R}^2}(|\mathscr{B}_n(\mathbf{k}')|)} |\mathscr{B}_n(\mathbf{k})| \,. \tag{5}$$

3. Examples and basic properties of the Bloch transform

We now illustrate some of the properties of the Bloch transform in the context of two examples. In both the MOFs are made out of a cladding of hexagonally packed air inclusions in silica, the core being defined by a missing hole.

Figure 1 shows an example of a mode of the symmetry class 1 of McIsaac [12], for two MOFs with different number of rings N_r but with same pitch (center to center distance) Λ and hole-diameter d ($\Lambda = 2.3\mu$m, $d/\Lambda = 0.15$), and at the same wavelength ($\lambda = 1.55\mu$m). The total Bloch transform shown was computed with the E_z Fourier-Bessel coefficients, but the transform is the same to graphical accuracy when computed with the coefficients related to H_z. The total Bloch transform indicates that both modes result from the superposition of 6 Bloch

#3960 - $15.00 US
Received 2 March 2004; revised 6 April 2004; accepted 8 April 2004

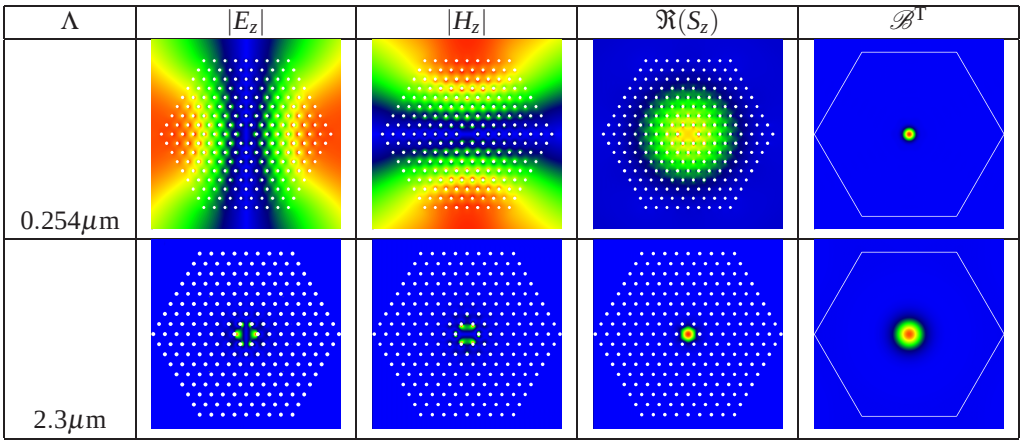

Fig. 2. Fundamental mode of two MOFs with different pitch, but with same $d/\Lambda = 0.3$ and $N_r = 8$. The field distribution changes considerably between the two values of the pitch, but the Bloch transform remains a single peak centered on the origin. For all figures $\lambda = 1.55\ \mu$m and $n_{\text{silica}} = 1.44402036$.

waves. Note that the Bloch vectors indicated by the peaks of the Bloch transform constitute symmetric pairs, and point in directions orthogonal to the last layer of holes of the cladding. This suggests that these modes consist of Bloch waves resonating between the borders of the MOF.

We see that for $N_r = 4$ the peaks in the Bloch transform are quite broad, and quite naturally become much narrower for $N_r = 10$. For $N_r = 4$, secondary peaks are not negligible; this exemplifies the importance of surface and defect effects for a system consisting of only 4 periodic layers. For $N_r = 10$ on the contrary, peaks are well defined, and the importance of secondary peaks is less, suggesting that edge effects are becoming negligible. In both cases the main peaks are close to the edge of the first Brillouin zone, indicating that each Bloch component is close to a standing wave. We note that the exact position of the maxima of the peaks is not the same in both cases, but that the "overall shape" remains constant. We further note the predicted periodicity in the reciprocal space of $\mathscr{B}^T(\mathbf{k})$: the peaks outside the first Brillouin zone are replicates of the peaks inside the first Brillouin zone, and do not contain any additional information. Finally, we note that the Bloch transform has symmetry properties induced by the symmetry properties of the mode.

Figure 2 shows a second example illustrating how helpful the Bloch transform becomes when trying to identify modes of MOFs having different yet comparable structures. Both lines of contour plots shown in Fig. 2 relate to the fundamental mode of a MOF with $N_r = 8$ holes of air inclusions in silica, with the same relative hole size $d/\Lambda = 0.3$ and at same wavelength $\lambda = 1.55\mu$m, but with different values of the pitch. We see that the field patterns differ considerably, but that the Bloch transform remains similar for the two values of the pitch: there is only one peak centered on $\mathbf{k} = 0$, only the width of the peak changes, being much narrower for the wider mode than for the well confined mode.

This example illustrates well the Heisenberg-type property of the Bloch transform, which relates to its definition as a finite Fourier transform (*cf* Section 4). The more localized a mode is in real space, the more spread out is its Bloch transform in reciprocal space.

The most striking property of the Bloch transform is that the geometric distribution of the peaks - the *"shape"* of the Bloch transform - is characteristic of a MOF mode, and is extremely stable when varying the wavelength or the fiber parameters. We found in our studies of mode

#3960 - $15.00 US
Received 2 March 2004; revised 6 April 2004; accepted 8 April 2004

transitions in MOFs [3, 4] that the field distributions and the Fourier-Bessel coefficients of the same mode can vary considerably with varying fiber parameters, and that it can become extremely difficult to identify similar modes of different yet comparable structures. Our simulations have shown that the Bloch transform of a given mode keeps its shape regardless of the fiber parameters, and that this shape is indeed the most precise and convenient way to differentiate and define specific modes. It is difficult to prove this property without precisely defining a classification of modes, but it can be understood through the fact that the Bloch transform decomposes each mode in a natural basis for the structure. In fact we can use this property as an axiom, defining the nature of a mode through the properties of its Bloch transform.

4. Advanced properties

We here consider a mode consisting of a superposition of a finite number N_{B} of Bloch waves so that Eq. (3) is satisfied.

4.1. Normalizing the Bloch transform: Bloch wave decomposition and Parseval identity

Until now we have only interpreted the location of peaks of the Bloch transform. However, through a correct normalization of the Bloch transform, the numerical value of $\mathscr{B}_n(\mathbf{k})$ can also be given a meaning.

First we make explicit the value of the Bloch transform when $\mathbf{k}$ takes the value of one of the Bloch vectors $\mathbf{k}_{\mathrm{B}}^m$ of the field:

$$\mathscr{B}_n(\mathbf{k}_{\mathrm{B}}^m) = \sum_{l=1}^{N_{\mathrm{i}}} \sum_{j=1}^{N_{\mathrm{B}}} \hat{B}_n^j \exp\left(i(\mathbf{k}_{\mathrm{B}}^m - \mathbf{k}_{\mathrm{B}}^j)\cdot \mathbf{c}_l\right) , \tag{6}$$

$$= N_{\mathrm{i}} \hat{B}_n^m + \sum_{j=1, j\neq m}^{N_{\mathrm{B}}} \hat{B}_n^j \sum_{l=1}^{N_{\mathrm{i}}} \exp\left(i(\mathbf{k}_{\mathrm{B}}^m - \mathbf{k}_{\mathrm{B}}^j)\cdot \mathbf{c}_l\right) . \tag{7}$$

The analysis below holds when the last term in Eq. (7) can be neglected compared to the first. It can be shown that this is so when,

$$\forall \mathbf{G} \in \mathscr{L}^*, \forall\, j \neq m,\ |\mathbf{k}_{\mathrm{B}}^m - \mathbf{k}_{\mathrm{B}}^j + \mathbf{G}| N_{\mathrm{i}}^{1/2} \Lambda \gtrsim 4. \tag{8}$$

The width of the FBZ being of the order of $2\pi/\Lambda$, Eq.(8) is equivalent to having the distance between peaks, normalised to the width of the FBZ, greater than $2/(\pi N_{\mathrm{i}}^{1/2})$. We will see in Eq. (14) that the normalized width of the peaks is of the order of $1.91/(\pi N_{\mathrm{i}}^{1/2})$ so that Eq. (8) is in fact equivalent to the requirement that the peaks associated with the different Bloch factors do not overlap. In that case, then

$$\mathscr{B}_n(\mathbf{k}_{\mathrm{B}}^m) \simeq N_{\mathrm{i}} \hat{B}_n^m . \tag{9}$$

The value of the Bloch transform taken at a Bloch vector $\mathbf{k}_{\mathrm{B}}^m$ gives therefore an approximation of the complex amplitude $\hat{B}_n^m$ of the associated Bloch wave component in Eq. (3). Nevertheless, because of linearity, only relative amplitudes in that decomposition have a physical meaning, it is necessary to be able to compare the amplitudes to each other. Mathematically speaking, we aim at obtaining

$$\frac{\hat{B}_n^m}{\left(\sum_{j=1}^{N_{\mathrm{B}}} |\hat{B}_n^j|^2\right)^{1/2}} . \tag{10}$$

Rather than using Eq. (9) to evaluate the sum in Eq. (10), it is easier and numerically more precise to use Parseval like identities, whose derivations follow lines similar to the derivation

#3960 - $15.00 US
Received 2 March 2004; revised 6 April 2004; accepted 8 April 2004

of Parseval identites for Fourier series. We have

$$\sum_{l=1}^{N_\mathrm{i}} |B_n(\mathbf{c}_l)|^2 = \frac{1}{\mathscr{A}_\mathrm{FBZ}} \iint_\mathrm{FBZ} |\mathscr{B}_n(\mathbf{k})|^2 d\mathbf{k} \simeq N_\mathrm{i} \sum_{i=1}^{N_\mathrm{B}} |\hat{B}_n^i|^2, \tag{11}$$

where $\mathscr{A}_\mathrm{FBZ}$ is the area of the FBZ. Here the first identity is rigorous, and the second is valid when Eq. (8) is satisfied.

4.2. Width of the Bloch transform peaks: Heisenberg-like uncertainty

We have noted on the examples that the width of the peaks centered on the Bloch vectors $\mathbf{k}_\mathrm{B}^m$ decreases with increasing cladding size. An analytic analysis of Bloch transform peaks shows that peaks corresponding to one Bloch wave of amplitude $\hat{B}_n$ and Bloch vector $\mathbf{k}_\mathrm{B}$ are of the form

$$|\mathscr{B}_n(\mathbf{k})| = |\hat{B}_n| \left| \frac{\sin(N_1(\mathbf{k}-\mathbf{k}_\mathrm{b})\cdot\mathbf{u}_1\Lambda/2)}{\sin((\mathbf{k}-\mathbf{k}_\mathrm{b})\cdot\mathbf{u}_1\Lambda/2)} \right| \left| \frac{\sin(N_2(\mathbf{k}-\mathbf{k}_\mathrm{b})\cdot\mathbf{u}_2\Lambda/2)}{\sin((\mathbf{k}-\mathbf{k}_\mathrm{b})\cdot\mathbf{u}_2\Lambda/2)} \right|, \tag{12}$$

where $\mathbf{u}_i$ denote the unitary vectors along the directions defined by the elementary vectors defining $\mathscr{L}$ and N_i the number of inclusions along these same directions (so that N_i is of the order of N_1N_2). The peaks of the Bloch transform along each direction are therefore of the same type as the function

$$f(x) = \begin{cases} \left| \frac{\sin(ax)}{\sin(x)} \right| & \text{if } x \neq m\pi, m \in \mathbb{Z} \\ |a| & \text{if } x = m\pi, m \in \mathbb{Z}\,. \end{cases} \tag{13}$$

This function has main peaks of value a for $x = m\pi,\ m \in \mathbb{Z}$, and for large values of a has half-width points at $x \simeq m\pi \pm 1.91/a$. The width δk_m of the peaks of the Bloch transform along $\mathbf{u}_m$ is thus given by

$$\delta k_m \simeq 2\frac{1.91}{N_m\Lambda}\,. \tag{14}$$

The result to be retained from this analysis is that the width of a Bloch transform peak along a given direction varies as the inverse of cladding width along that same direction.

In the above analysis, the mode was assumed to be a superposition of a finite number of Bloch waves. When this is not the case, *e.g.* when the mode is a surface or defect state, the relation has to be modified. In the case of a localized defect mode (*e.g.* the mode for $\Lambda = 2.3\,\mu$m in Fig. 2), the magnitude of the $B_n(\mathbf{c}_l)$ coefficients decays exponentially away from the defect. In that case only the $B_n(\mathbf{c}_l)$ coefficients associated with inclusions close to the defect contribute significantly to the Bloch transform. The analytical analysis leading to Eq. (14) shows that the Heisenberg relation (14) remains true in these cases if N_m is replaced by the number of inclusions on which the mode's fields are significant, so that (14) is in fact a relation between the spatial extent of the mode and the width of the Bloch transform peaks.

5. Discussion and conclusions

We have found the Bloch transform discribed above to be extremely valuable for studies of MOF modes. Its ability to analyse modes in terms of resonating Bloch waves let us gain considerable insights into the physics of MOF modes, allowed us to identify modes without ambiguitiy and made a clear-cut distinction between cladding and defect modes possible. Although the method has been designed and tailored with the multipole method in mind, it is applicable within the framework of any method capable of generating accurate distributions of the electric and magnetic fields in MOFs. We consider its use will be of great advantage in design studies of MOFs for a range of advanced applications.

This work was produced with the assistance of the Australian Research Council under the ARC Centres of Excellence Program.

#3960 - $15.00 US Received 2 March 2004; revised 6 April 2004; accepted 8 April 2004